Catalysis Today 174 (2011) 135–140

Contents lists available at ScienceDirect

Catalysis Today

journal homepage: www.elsevier.com/locate/cattod

Pd-integrated lanthanum-transition metal perovskites for methanol partial oxidation

Chia-Liang Li, Chien-Lin Wang, Yu-Chuan Lin*

Department of Chemical Engineering and Materials Science, Yuan Ze Fuel Cell Center, Yuan Ze University, 135 Yuan-Tung Rd., Chungli 32003, Taoyuan, Taiwan

ARTICLE INFO

Article history:
Received 1 October 2010
Received in revised form
30 December 2010
Accepted 21 January 2011
Available online 26 February 2011

Keywords:
Perovskite
Palladium
Methanol
Oxidation
Formaldehyde

ABSTRACT

Palladium integrated lanthanum-transition metal perovskites ($LaMnO_3$, $LaFeO_3$, and $LaCoO_3$) were employed in methanol partial oxidation to formaldehyde. The crystallinity of these perovskites remained unchanged by incorporating up to 5 mol% Pd cations into their respective frameworks. Such a cation replacement could yield a positive effect on particle size and catalyst reducibility. The Pd cation exists in perovskites mostly as Pd^{2+}. Under partial oxidation conditions, the reactivity and formaldehyde selectivity of Pd-free perovskites were relatively low compared to their Pd-impregnated counterparts. Most importantly, the reaction mechanism could be promoted diversely. For Pd-free perovskites, methanol combustion, methanol oxidation to syngas and water, and methanol dehydrogenation were found to be prominent. In contrast, methanol partial oxidation to formaldehyde and methanol dehydrogenation were the major pathways of Pd-integrated catalysts. Both reactions can be seen as major factors in the elevation of formaldehyde selectivity.

1. Introduction

Perovskite (ABO_3) is a versatile catalyst which has been used in numerous fields such as exhaust abatement, CO oxidation, and methane partial oxidation [1]. This can be attributed to its unique crystalline structure, ion mobility, and thermal stability.

Taking methane partial oxidation to syngas for example, various perovskites were used at high temperatures (usually above 1000 K) to produce syngas. Slagtern and Olsbye studied $LaMO_3$ (M = Rh, Ni, and Co) perovskites in this field [2]. Among them, $LaRhO_3$ displayed attracting activity and stability at 1073 K for a 120-h lifetime test. This is attributed to well dispersion of Rh particles in the perovskite framework [2]. Lago et al. investigated the influence of A-site element of $LnCoO_3$ (Ln = La, Pr, Nd, Sm, and Gd) [3]. The stability of reduced Co ion is proposed to be correlated with perovskite's activity and selectivity. Interestingly, with decreasing the ionic radii of the A-site element, yield of syngas can be improved [3]. Owing to the high electronic and ionic conductivity, perovskite-made membrane reactors, e.g., $LaCoO_3$ and $LaFeO_3$, were frequently employed in methane partial oxidation to syngas [1,4,5]. This design facilitates the reaction by oxygen permeation fluxes through perovskites, which allows safe operation and cost efficient air separation.

Recently, precious metals, such as Pd, Pt, and Rh, have been successfully embedded into perovskite for automotive-emission treatments [6–11]. These catalysts have shown surpassing reactivity and durability when compared to supported noble metal catalysts [6]. Among the precious metals, palladium is the most economic and demanding, particularly for uses in cold start emission reduction [7]. However, sintering of Pd particles has been a long-lasting challenge in both industrial practice and academic research. Incorporating palladium into perovskite framework is a promising way to circumvent this difficulty because the thermal stability of Pd species can be significantly enhanced. In addition, the perovskite framework may serve as an active support due to its unique lattice oxygen chemistry [1].

In comparison with NO_x reduction [12–14] and combustion [15–17], however, relatively fewer efforts have been dedicated to methanol partial oxidation to formaldehyde using Pd-integrated perovskites. De and Balasubramanian [18] employed $SrVO_3$ in methanol partial oxidation to formaldehyde. By injecting methanol pulses into an oxygen-free system, they showed that lattice oxygen in perovskite could assist methanol conversion. Under partial oxidation condition, great formaldehyde selectivity (more than 90%) could be obtained at 320 °C, however, the activity was quite low (~44% conversion). Choisnet et al. [19] explored methanol oxidation on $LaNiO_3$ with CO_2 as the major product. Based on series of catalyst characterization, they proposed that the B-site oxide, NiO, played an important role in total oxidation. Lately, Kuhn and Ozkan [20] used Sr- and Co-doped $LaFeO_3$ in methanol partial oxidation for hydrogen production. A comprehensive study through the variation of B-site element compositions was reported. Moreover, they elucidated how perovskite's chemistry could tune the

* Corresponding author.
E-mail address: yclin@saturn.yzu.edu.tw (Y.-C. Lin).

0920-5861/$ – see front matter © 2011 Elsevier B.V. All rights reserved.
doi:10.1016/j.cattod.2011.01.038

reaction mechanism. It is worth noting that formaldehyde was not detected in their system.

The objective of this study is to investigate the catalytic performance of Pd incorporated $LaBO_3$ (B = Mn, Fe, and Co) perovskites in the partial oxidation of methanol to formaldehyde. Both physical and chemical properties of perovskites were surveyed. Based on their catalytic behavior, plausible mechanisms processed via different perovskites were proposed. The current work shows the potential of Pd-impregnated perovskites in methanol partial oxidation.

2. Experimental

2.1. Catalyst preparation

Six samples, including $LaBO_3$ (B = Mn, Fe, and Co) and $LaB_{0.95}Pd_{0.05}O_3$ catalysts were prepared applying a sol–gel method reported elsewhere [21]. For convenience, $LaBO_3$ samples will henceforth referred to as LaB (e.g., LaMn) and $LaB_{0.95}Pd_{0.05}O_3$ were labeled as LaBPd (e.g., LaMnPd). A binary solution (260 ml), containing ethylene glycol and methanol in a 1-to-4 volumetric ratio, was used to dissolve metal acetylacetonates (acac) (La-, Mn-, Co-, Fe-, and Pd-$(acac)_3$) in appropriate stoichiometric ratios. About 10 mmol of A-site and B-site metal ions were used. After vigorous stirring for half an hour, the solution was transferred into a rotary evaporator at 80 °C. The temperature was maintained to remove solvents. The remaining paste was then collected and dried in air at 150 °C for 10 h using a heating rate of 10 °C/min. Finally, the dried sample was calcined with the same heating rate from 150 to 700 °C for 2 h.

2.2. Catalyst characterization

The surface areas were measured by an automated N_2 adsorption apparatus (Micromeritics, ASAP 2010). Before each trial, the sample was degassed at 105 °C for 6 h. Adsorption of N_2, a probe species, was performed at −196 °C. Surface areas of samples were calculated based on the method of Brunauer, Emmet, and Teller (BET).

Powder X-ray diffraction (XRD) patterns were obtained with a Shimadzu Labx XRD-6000 using Cu Kα radiation (0.15418 nm). Scans were conducted using 20–80° angle range (2θ) with a scanning rate of 4°/min. The voltage and current used were 40 kV and 30 mA, respectively. Crystallite sizes were measured by employing the Scherrer relation, $L = 0.9 \times \lambda/\beta \cos\theta$, where L is the crystallite size, λ is the wavelength of radiation, β is the broadening of the peak due to the small crystallites (rad 2θ), and θ is the corresponding angle of the diffraction peak. The full width at half-maximum (FWHM) of each perovskite was estimated based on its strongest diffraction peak. The instrumental broadening effect was found to be negligible by using the Warren's correction [22].

The surface elemental analysis was performed by an energy dispersive spectrometer (EDS, Oxford INCA Energy 350) attached to the field-emission scanning electron microscopy (FESEM, JEOL JSM-6701F). The INCA X-Sight software package (Oxford Instrument) was used to quantify elemental contents. Three trials with different positions were averaged for each sample. The acquisition time per location was 10 min. The SEM accelerating voltage was 10 kV. The scanned areas were ~4 μm × 3 μm. Elements including O, La, Mn, Fe, Co, and Pd were determined by EDS from their K-lines. X-ray photoelectron spectroscopy (XPS) analysis was conducted using a Kratos Axis Ultra DLD with a 180° hemispherical sector analyzer and a Al monochromator (X-ray sources: Mg and Al Kα source, 450W max power). The dwell time was 0.3 s. Correction of the energy shift due to the static charging of the samples was accomplished with the C 1s peak at 284.4 eV (adventitious carbon) as a reference.

H_2-temperature programmed reduction (H_2-TPR) and temperature programmed desorption (TPD) were conducted in a U-shaped quartz reactor (i.d. = 6 mm) surrounded by a temperature-controlled furnace. A water-trap and a thermal conductivity detector (TCD) were connected in series to record responses. For H_2-TPR runs, the TCD current was set at 50 mA and the detector's temperature was at 100 °C; for TPD experiments, the TCD current was 170 mA at 150°C. Approximately 50 mg of sample was used per trial. Prior to each experiment, the sample was pretreated in Ar (H_2-TPR, 23 ml/min) or He (TPD, 23 ml/min) at 120 °C (10 °C/min) for 30 min to remove physisorbed water. After cooling to room temperature, the H_2-TPR was performed in a 7.4% H_2/Ar stream (25 ml/min) by elevating the temperature to 900 °C with a 5 °C/min ramp rate. The TPD was conducted in a He stream with a heating rate of 5 °C/min from 100 to 925 °C, followed by isothermal soaking at 925 °C for 30 min.

2.3. Activity measurements

Catalytic performance was tested in a continuous fixed bed reactor (i.d. = 10 mm). The system outlet was connected inline to a gas chromatograph (GC, SRI 8610) equipped with a TCD, a methanizer, and a flame ionization detector (FID). Ultra-high purity Ar was used as the carrier gas. Before each trial, the catalyst was treated in a 10% O_2/N_2 stream at 700 °C for an hour using a 10 °C/min heating rate from room temperature. A 5 Å molecular sieve and Porapak Q columns were used to separate reactants and products. Identified effluents included N_2, CO, CO_2, H_2, HCOH, CH_3OH and trace CH_4. No formic acid or methyl formate was detected. N_2 also served as the internal standard. All products except H_2O were measured relative to GC calibration standards. The amount of H_2O was estimated by an oxygen atom balance. Approximately 0.1 g of sample with particle sizes ranging from 40 to 80 mesh was employed. A K-type thermocouple was inserted in the middle of catalyst bed from the rear end of reactor to record the reaction temperature.

Methanol was introduced into the system through a syringe pump (New Era, NE-300) at an injection rate of 1 ml/h. All tubing of the system was wrapped with heating tape and kept at 150 °C to avoid condensation. The molar composition of the feed was $CH_3OH/O_2/N_2 = 11/5/84$ with a fixed residence time of 4.1 g catalyst × h/mol of CH_3OH. For all trials, the carbon atom mass balances were within ±10% error, mostly less than ±5%. For each data point, three trials were taken after reaching the steady-state of the system (about 30 min after start-up). These trials were employed to estimate 95% confidence intervals for both conversion and selectivity. The conversion was calculated as mole of methanol reacted divided by mole of methanol injected. The selectivities of carbon containing products (CO, CO_2, and HCOH) were calculated based on carbon atoms. The selectivities of H_2 and H_2O were calculated based on hydrogen atoms.

3. Results and discussion

Fig. 1 shows the XRD patterns of perovskites. The characteristic reflections of LaMn ([JCPDS: 35-1353]), LaFe ([JCPDS: 37-1493]), and LaCo ([JCPDS: 48-0123]) were well defined. The diffraction patterns of Pd-embedded samples were nearly identical to their corresponding perovskite structures. This suggests that up to 5 mol% Pd ions could be placed in the B-site position of the lanthanum-based perovskite while its crystallinity could be maintained. Another possible explanation may be attributed to small PdO clusters, which was below the XRD detection limit (ca. 4 nm), on the catalyst surface. A close look of the XRD patterns showed

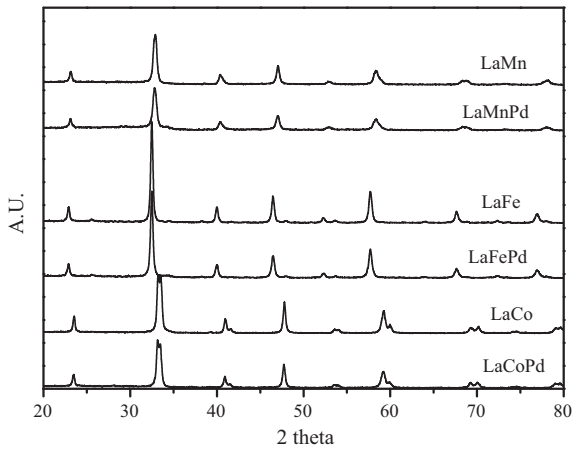

Fig. 1. XRD patterns of the lanthanum-based perovskites.

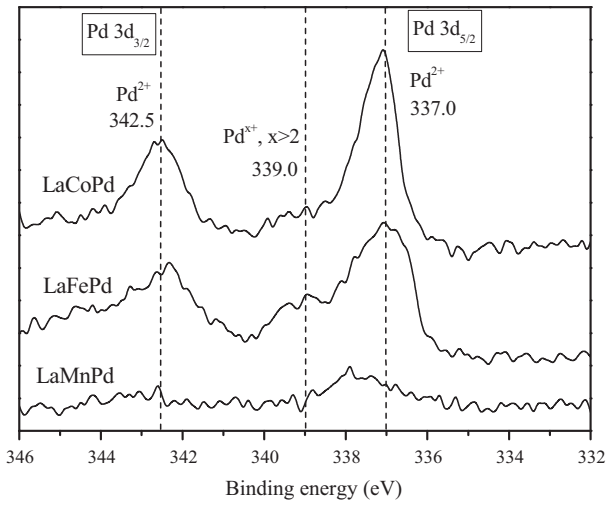

Fig. 2. Evolution of Pd 3d XPS of Pd-incorporated perovskites.

slight shift toward higher 2θ degree for Pd-doped perovskites. According to Bragg's law [23], this implies the decrease in *d*-spacing by the Pd substitution. Table 1 lists surface areas and particle sizes of all perovskites. Surface areas of all samples were close, ranging from 1.4–6.6 m^2/g. LaCo based catalysts yielded the smallest particle size, whereas LaFe perovskites had the largest crystallite size. Particle diameters were in the range of 13–29 nm. Note that the addition of Pd ions into the perovskite framework had a positive effect in dwindling crystallite size.

Table 1 summarizes the EDS analysis of surface compositions. The grain morphologies recorded by FESEM were irregular (see Supplementary data, Fig. S1). EDS results showed a close match of their nominal compositions. The exceptions were LaMn and LaMnPd; the Mn-to-La ratios of these two were 0.53 and 0.33, respectively. These values, which lower than Mn/La stoichiometric numbers of perovskites, imply possible surface enrichment of La [24,25].

Fig. 2 illustrates the XPS analysis of Pd states of freshly synthesized LaMnPd, LaFePd, and LaCoPd. The metallic Pd peak, which is located at 335.2 eV [26], was absent for all samples. Two major peaks corresponding to Pd $3d_{5/2}$ (337.0 eV) and Pd $3d_{3/2}$ (342.5 eV) were recognized. Both of these two can be attributed to oxidized Pd^{2+} [7,27,28]. Among all Pd-integrated perovskites, LaMnPd displayed a weaker response than LaFePd and LaCoPd, even though all three had the same Pd loading. This confirms the EDS result, which suggests the inhomogeneous LaMnPd surface. At around 339.0 eV, a shoulder could be observed on the spectra of LaFePd and LaCoPd. This characteristic signal is ascribed to higher oxidized Pd^{x+} ($x = 3$ and/or 4), particularly for B-site substituted perovskites [27–29]. Comparing the Pd^{x+} signals of LaFePd and LaCoPd using their Pd $3d_{5/2}$ peaks (337.0 eV) as basis, the former was slightly stronger than the latter. In other words, LaFePd might possess higher Pd^{x+}/Pd^{2+} ratio than LaCoPd. For LaMnPd, the response of Pd^{x+} was negligible. The differences in Pd oxidation states were reported to be an important issue in varying catalytic performances, for example, the three-way catalyst [28].

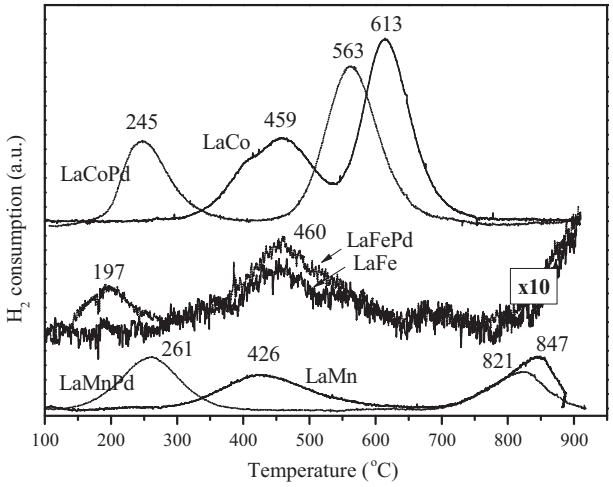

Fig. 3. H_2-TPR profiles of LaMn, LaFe, and LaCo based perovskites. Note that signals of both LaFe and LaFePd were multiplied by a factor 10.

Fig. 3 depicts the H_2-TPR profile of each sample. LaFe based perovskites showed comparatively weak H_2 consumption responses, which is consistent with recent studies [17,30,31]. That is, LaFe and LaFePd perovskites were both difficult to be reduced. The XRD patterns of post-TPR LaFe and LaFePd samples (see Supplementary data, Fig. S2 and S3) show almost identical responses as their perovskite states. This is in agreement with the H_2-TPR studies of LaFe based perovskites. To clarify, signals of LaFe based perovskites were multiplied by a factor 10. Besides LaFe, all perovskites showed two different peaks.

The H_2-TPR profiles of LaMn-, LaFe-, and LaCo-based perovskites were highly convoluted, rendering ambiguous reduction mechanisms of these solid solutions. Generally, their reduction processes

Table 1
Physicochemical properties of catalysts used in this study.

Catalyst	S_{BET} (m^2/g)	d_p (nm)	La[a]	Mn[a]	Fe[a]	Co[a]	Pd[a]	O[a]	Mn/La	Fe/La	Co/La	Pd/La
LaMn	6.3	16.6	25.3	13.4	–	–	–	61.3	0.53	–	–	–
LaFe	6.6	28.5	21.4	–	20.1	–	–	58.5	–	0.94	–	–
LaCo	3.7	13.4	21.5	–	–	20.2	–	58.3	–	–	0.94	–
LaMnPd	1.4	14.8	27.9	9.2	–	–	2.3	60.6	0.33	–	–	0.08
LaFePd	5.7	24.4	19.7	–	21.9	–	0.6	57.9	–	1.11	–	0.03
LaCoPd	3.9	13.0	24.0	–	–	19.3	0.6	56.2	–	–	0.80	0.03

[a] Obtained by EDS analysis.

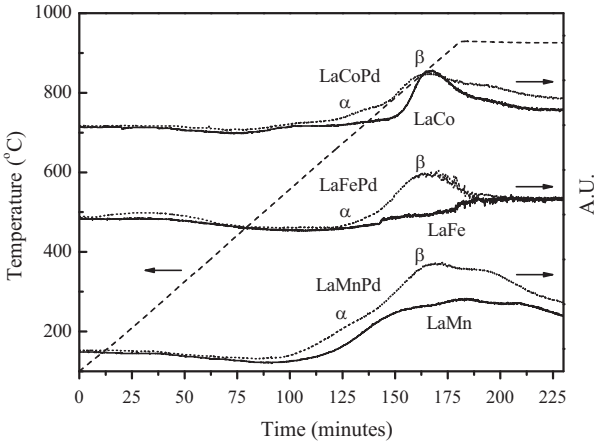

Fig. 4. TPD profiles of LaMn, LaFe, and LaCo based perovskites. The dash line represents the desorption temperature.

have been widely accepted to follow a multiple-step mechanism. Regarding LaMn based perovskites, Mn^{4+} and Mn^{3+} may coexist prior to the reduction. After the reduction, Mn^{2+} instead of Mn^0 should be the final state of Mn ions [32]. This is also the case for LaFe, which may hold both Fe^{4+} and Fe^{3+} at the initial state; whereas both Fe^{2+} and metallic iron could be the reduced states of Fe ions [30]. For LaCo, the first peak presents Co^{3+} reduction into Co^{2+} to form brownmillerite ($LaCoO_{2.5}$), followed by the second reduction of Co^{2+} to metallic cobalt [33,34]. Controversially, a single-step reduction mechanism (Co^{3+} to Co^0) was reported by Huang and coworkers [35], arguing that separated TPR peaks and unsymmetrical patterns should be attributed to differences of crystalline sizes and oxygen defects in the perovskite lattice. Such diverse structures may lead to various diffusion resistances during hydrogen reduction, thereby varying TPR profiles [35,36].

The shift of reduction peaks toward lower temperatures by doping Pd ions into LaMn, LaFe, and LaCo implies that the reducibility of perovskites can be substantially enhanced. For LaMnPd, the first peak shifted from 426 to 261 °C while the second peak shifted from 847 to 821 °C. A newly formed response at 197 °C was discovered for LaFePd. The first peak of LaCoPd decreased from 459 to 245 °C while the second peak decreased from 613 to 563 °C. It is acknowledged that hydrogen can dissociatively adsorb on Pd clusters, which already reduced at low temperature region, and spillover to the support [37–40]. The spillover can facilitate the reduction of supports, resulting in low reduction temperature of Pd-integrated perovskites [38–40]. In addition, dosing trace Pd ions into perovskites could increase the low temperature reduction peak area, except for LaCoPd. This could be explained by either increasing amount of small crystallites or defects of lattice structure [35,36], or hydrogen spillover effect [37–40]. It is worth noting that the reduction of PdO, which mostly occurs at about 100 °C [37,41], was not observed. This again reveals that Pd ions could be well embedded into the perovskite framework, resulting in the absence of a segregated peak caused by PdO reduction.

Fig. 4 shows the TPD profiles of LaMn-, LaFe-, and LaCo-based perovskites. In general, desorbed oxygen of perovskites can be classified into two types: α- and β-oxygen. The former has been assigned to weakly bonded oxygen species on perovskite surfaces; the latter has been known as the lattice oxygen in perovskite frameworks [41,42]. Naturally, the weakly bonded α-oxygen can be released at relatively lower temperature compared to rigidly bonded β-oxygen. Temperatures ranging from 700 to 800 °C have been employed as the demarcation between these two [42–44]. Both types of oxygen species play an important role in various oxidation reactions [45]. For example, α-oxygen may promote combustion while β-oxygen is proposed to be responsible for partial oxidation [43]. In Fig. 4, the amounts of α- and β-oxygen could be greatly improved by substituting Pd ions into perovskite frameworks. This implies that the reactivities of LaMn, LaFe, and LaCo perovskites could be enhanced by the Pd substitution, in agreement with aforementioned H_2-TPR studies.

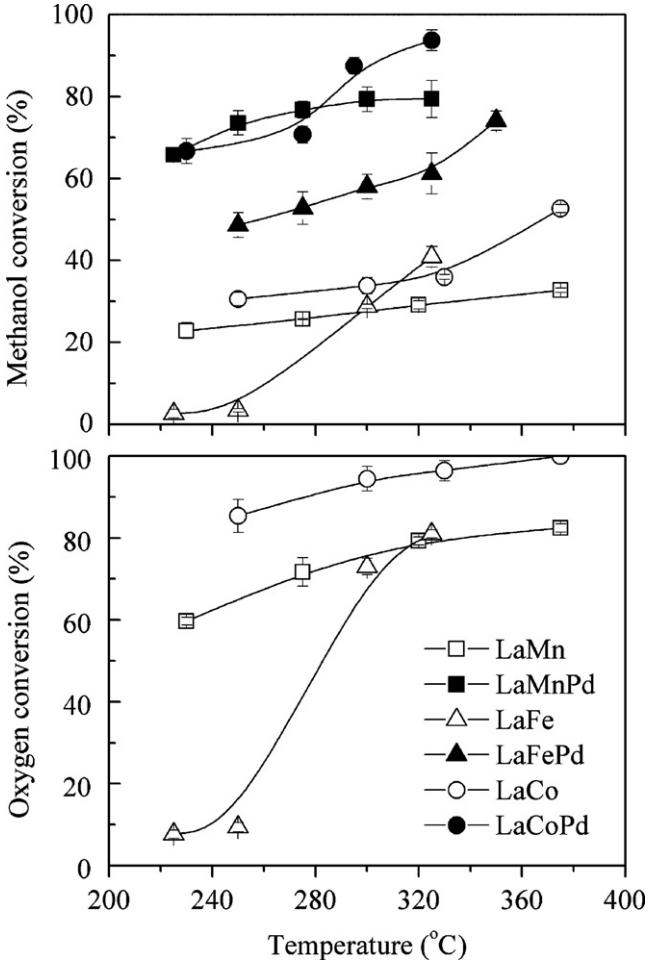

Fig. 5. Methanol and oxygen conversions as a function of temperature. Note for Pd-incorporated perovskites, oxygen conversions are all at 100%.

Fig. 5 displays methanol and oxygen conversions as a function of reaction temperature. Incorporating 5 mol% Pd ions could substantially increase activities of perovskites. At equivalent temperatures, Pd-doped perovskites were more than twice reactive as their Pd-free counterparts. For instance, LaMnPd possessed about 63% conversion at 220 °C, which was three times higher than LaMn. This trend is in accord with previous H_2-TPR results: the Pd-integrated perovskites had greater reducibilities than their Pd-free counterparts. The activities of all samples could be enhanced by elevating their respective temperatures. For Pd-free perovskites, increasing the temperature could enhance both methanol and oxygen conversions. Oxygen was fully consumed for Pd-doped perovskites over the entire range of reaction temperature. The order of increasing activity was LaFePd < LaMnPd < LaCoPd. At about 330 °C, the most active LaCoPd could achieve more than 90% methanol conversion. LaFePd was ranked as the least active catalyst among Pd-doped perovskites. Interestingly, however, its Pd 3d XPS profile displayed a stronger response than LaMnPd. This implies that instead of surface Pd species content, the reducibility of the perovskite (as shown in H_2-TPR) and/or oxidation states of Pd were the major factors for catalytic activity.

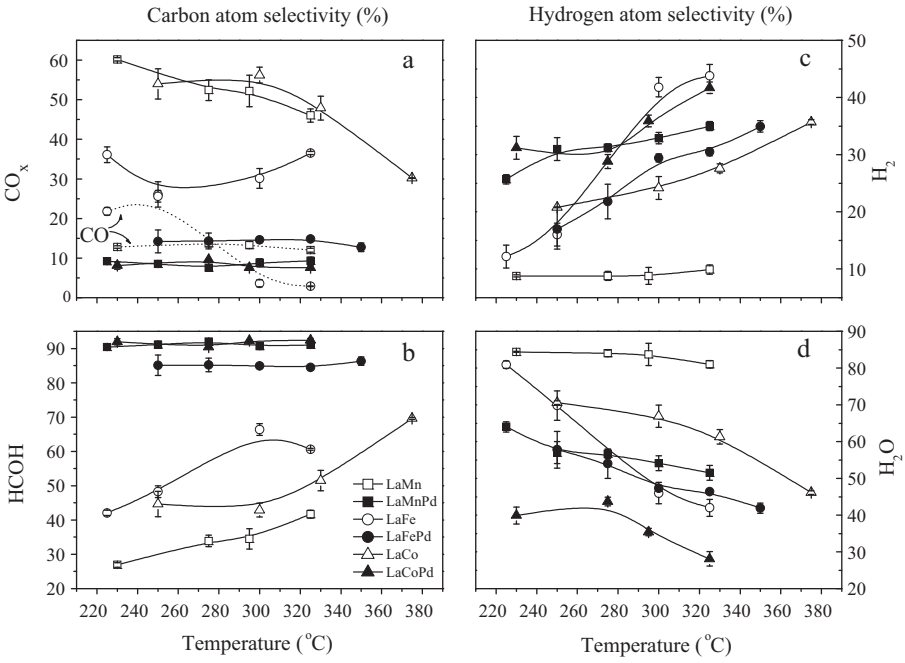

Fig. 6. Selectivity of (a) CO_x (solid line, CO_2; dash line, CO), (b) HCOH, (c) H_2, and (d) H_2O as a function of temperature.

Fig. 6 illustrates both carbon and hydrogen atom selectivities as a function of reaction temperature. In Fig. 6(a), CO and CO_2 selectivities displayed quite different results. LaMn and LaFe were the only two catalysts producing a considerable amount of CO. With increasing temperature, the CO selectivity of LaFe fell but was almost unchanged for LaMn. No CO was produced through the use of LaCo. CO_2 fell steadily with increasing temperature for LaMn and LaCo, whereas no clear trend was identified for LaFe. As for the Pd-containing perovskites, no CO could be generated; selectivities of CO_2 were nearly unaltered with increasing temperature. Fig. 6(b) illustrates formaldehyde selectivity as a function of temperature. Pd-free perovskites enhanced formaldehyde selectivity with increasing temperature. The highest selectivity of formaldehyde was about 70% at 375 °C by LaCo. For Pd-incorporated perovskites, formaldehyde selectivity was insensitive to reaction temperature. The order of increasing formaldehyde selectivity was: LaFePd (~85%) < LaMnPd (~90%) ~ LaCoPd (~90%). Again, no significant changes were identified for Pd-doped catalysts. Note that about two to three folds more formaldehyde could be generated by Pd-incorporated perovskites than their Pd-free counterparts. Fig. 6(c) and (d) shows both H_2 and H_2O selectivities as the function of temperature. All catalysts except LaMn displayed similar trends: enhancing temperature resulted in increasing H_2 and decreasing H_2O selectivities.

Scheme 1 lists the possible reactions under methanol oxidation condition [20,46,47]. For Pd-free perovskites, the major reaction pathway at low temperature was methanol combustion, which could be explained by high CO_2 and H_2O selectivities. By elevating temperature, highly exothermic combustion could be suppressed. The increasing HCOH and H_2 together with decreasing H_2O suggest dehydrogenation was promoted even when oxygen was still available. It is surprising that CO could be yielded so considerably by LaMn (~12%) and LaFe (~21%) at the low temperature region. A possible explanation might be ascribed to methanol decomposition, formaldehyde decomposition, or methanol oxidation to syngas and water [20]. Since methanol decomposition is thermodynamically unfavorable to proceed at this low temperature regime [47] and formaldehyde increased with elevating temperature, oxidation of methanol to syngas and water might be the major factor for CO production.

Incorporating Pd ions into perovskites varied the reaction scheme of methanol partial oxidation substantially. Formaldehyde is the major product with trace CO_2. This implies that the influence from combustion was limited. At low temperature, selectivities of H_2O were slightly higher than H_2, suggesting methanol partial oxidation to formaldehyde was preferred. With elevating temperature, the increasing H_2 and declining H_2O implies methanol dehydrogenation was gradually enhanced with fading partial oxidation. Even though oxygen was totally consumed, the selectivity of formaldehyde seemed to be insensitive to reaction temper-

Partial oxidation of methanol to formaldehyde:

$$CH_3OH + 1/2O_2 \rightarrow HCOH + H_2O \ (\Delta H = -159 \text{ kJ/mol})$$

Methanol dehydrogenation:

$$CH_3OH \rightarrow HCOH + H_2 \ (\Delta H = +84 \text{ kJ/mol})$$

Methanol oxidation to syngas and water:

$$CH_3OH + 1/2O_2 \rightarrow CO + H_2 + H_2O \ (\Delta H = -151 \text{ kJ/mol})$$

Methanol combustion:

$$CH_3OH + 3/2O_2 \rightarrow CO_2 + 2H_2O \ (\Delta H = -674 \text{ kJ/mol})$$

Methanol decomposition:

$$CH_3OH \rightarrow CO + 2H_2 \ (\Delta H = +91 \text{ kJ/mol})$$

Formaldehyde combustion:

$$HCOH + O_2 \rightarrow CO_2 + H_2O \ (\Delta H = -514 \text{ kJ/mol})$$

Partial oxidation of formaldehyde:

$$HCOH + 1/2O_2 \rightarrow CO_2 + H_2 \ (\Delta H = -271 \text{ kJ/mol})$$

Formaldehyde decomposition:

$$HCOH \rightarrow CO + H_2 \ (\Delta H = +12 \text{ kJ/mol})$$

Hydrogen combustion :

$$H_2 + 1/2O_2 \rightarrow H_2O \ (\Delta H = -243 \text{ kJ/mol})$$

Scheme 1. Plausible reactions under methanol oxidation condition.

ature. This is evidenced by the fact that incorporated Pd ions promoted methanol partial oxidation at low temperature, and promoted dehydrogenation at high temperatures. Both partial oxidation and dehydrogenation could contribute to formaldehyde yields.

The influence of B-site ions in Pd-free perovskites is highly complicated. It is unclear at this stage whether to correlate perovskite nature with its catalytic behavior. However, by doping trace Pd cations, partial oxidation and dehydrogenation of methanol to formaldehyde became two major pathways. A close inspection of catalytic activities together with XPS spectra showed that the least active LaFePd had the highest Pd^{x+}-to-Pd^{2+} ratio. Such a trend was also reported when applying Pd-containing perovskites as three-way catalysts for CO, NO and CH_4 abatement [28]. It is plausible that the same could be stated in the partial oxidation of methanol to formaldehyde.

4. Conclusion

The chemistry and catalytic performance of lanthanum-transition metal perovskites can be substantially altered by dissolving trace Pd cations in their crystalline frameworks. The presented information led to following conclusions:

1. The perovskite structure could be maintained by substituting up to 5 mol% B-site (Mn, Fe, and Co) elements with Pd cations. Segregated PdO was not observed. The positive effect on crystalline size was discovered when impregnating Pd cations into perovskites.
2. Reducibilities and oxygen desorption of La-based perovskites, which are highly related to catalytic activities, were improved by incorporated Pd cations. Pd species exist in perovskites mostly as oxidized Pd^{2+}; relatively less Pd^{3+} or Pd^{4+} could be identified. The former is proposed to be more active in methanol partial oxidation than the latter.
3. Besides methanol partial oxidation to formaldehyde, methanol combustion and methanol oxidation to syngas and dehydrogenation were found on Pd-free perovskites. In contrast, partial oxidation to formaldehyde and dehydrogenation were the two favored pathways on Pd-doped perovskites. Formaldehyde selectivities were insensitive to reaction temperature, ranging from 85% to 92% within the entire temperature region for Pd-doped perovskites.

Acknowledgements

This work was sponsored by the National Science Council of Taiwan under grant #NSC 98-2218-E-155-006. Valuable suggestions of Prof. C.-T. Yeh (Yuan Ze University) and anonymous reviewers are gratefully appreciated.

Appendix A. Supplementary data

Supplementary data associated with this article can be found, in the online version, at doi:10.1016/j.cattod.2011.01.038.

References

[1] M.A. Peña, J.L.G. Fierro, Chem. Rev. 101 (2001) 1981.
[2] Å. Slagtern, U. Olsbye, Appl. Catal. A 110 (1994) 99.
[3] R. Lago, G. Bini, M.A. Peña, J.L.G. Fierro, J. Catal. 167 (1997) 198.
[4] Y.H. Hu, E. Ruckenstein, Adv. Catal. 48 (2004) 297.
[5] B. Christian Enger, R. Lødeng, A. Holmen, Appl. Catal. A 346 (2008) 1.
[6] Y. Nishihata, J. Mizuki, T. Akao, H. Tanaka, M. Uenishi, M. Kimura, T. Okamoto, N. Hamada, Nature 418 (2002) 164.
[7] H. Tanaka, Catal. Surv. Asia 9 (2005) 63.
[8] H. Tanaka, M. Taniguchi, M. Uenishi, N. Kajita, I. Tan, Y. Nishihata, J. Mizuki, K. Narita, M. Kimura, K. Kaneko, Angew. Chem. Int. Ed. 45 (2006) 5998.
[9] H. Tanaka, M. Uenishi, M. Taniguchi, I. Tan, K. Narita, M. Kimura, K. Kaneko, Y. Nishihata, J. Mizuki, Catal. Today 117 (2006) 321.
[10] M. Taniguchi, H. Tanaka, M. Uenishi, I. Tan, Y. Nishihata, J. Mizuki, H. Suzuki, K. Narita, A. Hirai, M. Kimura, Top. Catal. 42–43 (2007) 367.
[11] M. Misono, Catal. Today 144 (2009) 285.
[12] A. Ueda, Y. Yamada, M. Katsuki, T. Kiyobayashi, Q. Xu, N. Kuriyama, Catal. Commun. 11 (2009) 34.
[13] G.C. Mondragón Rodriguez, B. Saruhan, O. Petrova, W. Grünert, Top. Catal. 52 (2009) 1723.
[14] J. Zhu, A. Thomas, Appl. Catal. B 92 (2009) 225.
[15] S. Specchia, P. Palmisano, E. Finocchio, M.A.L. Vargas, G. Busca, Appl. Catal. B 92 (2009) 285.
[16] N. Russo, P. Palmisano, D. Fino, Top. Catal. 52 (2009) 2001.
[17] A. Eyssler, P. Mandaliev, A. Winkler, P. Hug, O. Safonova, R. Figi, A. Weidenkaff, D. Ferri, J. Phys. Chem. C 114 (2010) 4584.
[18] K.S. De, M.R. Balasubramanian, J. Catal. 81 (1983) 482.
[19] J. Choisnet, N. Abadzhieva, P. Stefanov, D. Klissurski, J.M. Bassat, V. Rives, L. Minchev, J. Chem. Soc. Faraday Trans. 90 (1994) 1987.
[20] J.N. Kuhn, U.S. Ozkan, J. Catal. 253 (2008) 200.
[21] Y. Shimizu, T. Murata, J. Am. Ceram. Soc. 80 (1997) 2702.
[22] B.E. Warren, J. Appl. Phys. 12 (1941) 375.
[23] W.L. Bragg, Proc. Cambridge Philos. Soc. 17 (1913) 43.
[24] P.G. Menon, T.S.R.P. Rao, Catal. Rev.-Sci. Eng. 20 (1979) 97.
[25] B. Kucharczyk, W. Tylus, Catal. Today 137 (2008) 318.
[26] D. Briggs, M.P. Seah, Practical Structure Analysis, John Wiley, Chichester, 1993.
[27] M. Uenishi, M. Taniguchi, H. Tanaka, M. Kimura, Y. Nishihata, J. Mizuki, T. Kobayashi, Appl. Catal. B 57 (2005) 267.
[28] E. Tzimpilis, N. Moschoudis, M. Stoukides, P. Bekiaroglou, Appl. Catal. B 84 (2008) 607.
[29] J.M. Giraudon, A. Elhachimi, F. Wyrwalski, S. Siffert, A. Aboukaïs, J.F. Lamonier, G. Leclercq, Appl. Catal. B 75 (2007) 157.
[30] P. Ciambelli, S. Cimino, L. Lisi, M. Faticanti, G. Minelli, I. Pettiti, P. Porta, Appl. Catal. B 33 (2001) 193.
[31] J.P. Dacquin, M. Cabié, C.R. Henry, C. Lancelot, C. Dujardin, S.R. Raouf, P. Granger, J. Catal. 270 (2010) 299.
[32] L. Lisi, G. Bagnasco, P. Ciambelli, S. De Rossi, P. Porta, G. Russo, M. Turco, J. Solid State Chem. 146 (1999) 176.
[33] T. Nakamura, T. Petzov, L.J. Gauckler, Res. Bull. 14 (1979) 649.
[34] M. Crespin, W.K. Hall, J. Catal. 69 (1981) 359.
[35] L. Huang, M. Bassir, S. Kaliaguine, Appl. Surf. Sci. 243 (2005) 360.
[36] R.M. Navarro, M.C. Alvarez-Galvan, J.A. Villoria, I.D. González-Jiménez, F. Rosa, J.L.G. Fierro, Appl. Catal. B 73 (2007) 247.
[37] W.-J. Shen, M. Okumura, Y. Matsumura, M. Haruta, Appl. Catal. A 213 (2001) 225.
[38] K. Zhou, H. Chen, Q. Tian, Z. Hao, D. Shen, X. Xu, J. Mol. Catal. A 189 (2002) 225.
[39] L. Giebeler, D. Kießling, G. Wendt, Chem. Eng. Technol. 30 (2007) 889.
[40] W. Yao, R. Wang, X. Yang, Catal. Lett. 130 (2009) 613.
[41] R. Zhang, H. Alamdari, S. Kaliaguine, J. Catal. 242 (2006) 241.
[42] B. Levasseur, S. Kaliaguine, Appl. Catal. A 343 (2008) 29.
[43] T. Seiyama, N. Yamazoe, K. Eguchi, Ind. Eng. Chem. Prod. Res. Dev. 24 (1985) 19.
[44] S. Kaliaguine, A. Van Neste, V. Szabo, J.E. Gallot, M. Bassir, R. Muzychuk, Appl. Catal. A 209 (2001) 345.
[45] W.C. Conner, S. Soled, A. Signorelli, International Congress of Catalysis, Tokyo, Japan, 1981.
[46] G.I.N. Waterhouse, G.A. Bowmaker, J.B. Metson, Appl. Catal. A 265 (2004) 85.
[47] K.L. Hohn, Y.-C. Lin, ChemSusChem 2 (2009) 927.